# Beta-decay half-lives at the N = 28 shell closure

S. Grévy, J.C. Angélique, P. Baumann, C. Borcea, A. Buta, G. Canchel, W.N. Catford, S. Courtin, J.M. Daugas, F. de Oliveira, et al.

# Beta-decay half-lives at the $N = 28$ shell closure

S. Grévy [a,*], J.C. Angélique [a], P. Baumann [b], C. Borcea [c], A. Buta [c], G. Canchel [b],
W.N. Catford [d,a], S. Courtin [b], J.M. Daugas [e], F. de Oliveira [e], P. Dessagne [b], Z. Dlouhy [f],
A. Knipper [b], K.L. Kratz [g], F.R. Lecolley [a], J.L. Lecouey [a], G. Lehrsenneau [b],
M. Lewitowicz [e], E. Liénard [a], S. Lukyanov [h], F. Maréchal [b], C. Miehé [b], J. Mrazek [f],
F. Negoita [c], N.A. Orr [a], D. Pantelica [c], Y. Penionzhkevich [h], J. Péter [a], B. Pfeiffer [g],
S. Pietri [a], E. Poirier [b], O. Sorlin [i], M. Stanoiu [e,1], I. Stefan [c], C. Stodel [e], C. Timis [a,2]

[a] *Laboratoire de Physique Corpusculaire de Caen, IN2P3-CNRS, ENSICAEN et Université de Caen, F-14050 Caen cedex, France*
[b] *IReS, IN2P3/ULP, 23 rue du Loess, BP20, F-67037 Strasbourg, France*
[c] *Institute of Atomic Physics, IFIN-HH, Bucharest-Magurele, P.O. Box MG6, Romania*
[d] *Department of Physics, University of Surrey, Guildford, Surrey, GU2 7XH, UK*
[e] *GANIL, CEA/DSM-CNRS/IN2P3, BP5027, F-14076 Caen cedex, France*
[f] *Nuclear Physics Institute, AS CR, CZ-25068 Rez, Czech Republic*
[g] *Institut für Kernchemie, Universität Mainz, D-6500 Mainz, Germany*
[h] *FLNR, JINR, 141980 Dubna, Moscow region, Russia*
[i] *Institut de Physique Nucléaire, IN2P3-CNRS, F-91406 Orsay cedex, France*

## Abstract

Measurements of the beta-decay half-lives of neutron-rich nuclei (Mg–Ar) in the vicinity of the $N = 28$ shell closure are reported. Some 22 half-lives have been determined, 12 of which for the first time. Particular emphasis is placed on the results for the Si isotopes, the half-lives of which have been extended from $N = 25$ to 28. Comparison with QRPA calculations suggests that $^{42}$Si is strongly deformed. This is discussed in the light of a possible weakening of the spin–orbit potential.
© 2004 Elsevier B.V. Open access under CC BY license.

*PACS:* 21.10.Tg; 23.40.-s; 27.30.+t; 27.30.+z

*Keywords:* Lifetimes; Beta decay

---

## 1. Introduction

The investigation of very neutron-rich nuclei provides a fertile testing ground for our understanding of nuclear structure. In the region of $N = 28$, evidence has accumulated for modifications in the shell structure. In particular, the energies and $B(E2)$ for the lowest $J^\pi = 2^+$ states of the neutron-rich isotopes $^{38,40,42,44}$S, have been measured via Coulomb excitation [1,2] and indicate that $^{40,42,44}$S are moderately deformed ($|\beta_2| \approx 0.3$). These results support an earlier suggestion, derived from $\beta$-decay half-life and delayed-neutron emission probability measurements [3], of a weakening of the $N = 28$ shell closure below $^{48}$Ca. Mass measurements have provided additional evidence through the observation of a drop in the two-neutron separation energies ($S_{2n}$) at $N = 26$ instead of $N = 28$ for the S and P isotopic chains [4]. Furthermore the observation of an isomeric state in $^{43}$S pointed towards the presence of shape coexistence in the vicinity of $N = 28$ [4]. More detailed information on the level structures of the S and Ar nuclei was recently obtained from in-beam gamma spectroscopy experiments employing high-energy fragmentation [5, 6]. In particular the energies of the $4_1^+$ states in $^{46}$Ar and in $^{40,42}$S as well as those of the second $2^+$ states in $^{46}$Ar and in $^{40,42,44}$S were determined. It was concluded that $^{40}$S and $^{42}$S are deformed $\gamma$-soft nuclei, while $^{44}$S exhibits shape mixing in the low-lying states. Moreover it was concluded that the $N = 28$ shell gap was not large enough to compete against deformation.

Relativistic mean field calculations [7,8], Hartree–Fock calculations employing different Skyrme forces [9,10], and the Gogny interaction [11,12], as well as recent Hartree–Fock–Bogoliubov calculations using the SLy4 Skyrme interaction [13] predict both prolate and oblate deformed minima in the potential-energy surfaces for $^{44}_{16}$S$_{28}$. The nucleus $^{42}_{14}$Si$_{28}$ is calculated to be strongly oblate deformed by several models [7, 11,12]. This was interpreted as a consequence of a gradual reduction of the size of the $N = 28$ shell gap from $Z = 20$ to 14. Large scale shell model calculations by Retamosa et al. [14] are in good agreement with the experimental $B(E2)$ values for $^{40,42,44}$S. They concluded that an erosion of the $N = 28$ gap occurs for the sulfur isotopes with a maximum

deformation occurring in $^{42}$S. Moreover, the slope of the two-neutron separation energy for the Si isotopes together with the $2_1^+$ energy and the $\nu f_{7/2}$ occupation number indicate that the $^{42}$Si has the characteristics of a doubly magic nucleus, such as $^{48}$Ca. Recently the same authors adjusted the interaction to reproduce the single-particle states in $^{35}$Si [15] and interpreted the reduction between the $\nu f_{7/2}$ and $\nu p_{3/2}$ orbitals as an erosion of the spin–orbit force far from stability. This erosion is moderate and the changes at $N = 28$ are predicted to be very small except in the case of $^{42}$Si where the doubly closed-shell character is less pronounced in comparison with that found in Ref. [14] with the $2^+$ energy decreasing from 2.56 to 1.49 MeV. As such, the structure of $^{42}$Si appears to be quite sensitive to the choice of the interaction.

With present day detection arrays, nuclear structure studies via $\beta$-decay are feasible for relatively weakly produced nuclei lying far from stability (such as $^{42}_{14}$Si$_{28}$). For example, it has already been demonstrated that valuable nuclear structure information can be obtained from half-lives ($T_{1/2}$) and delayed-neutron emission probabilities ($P_n$) [3]. In particular, it was shown that the Gamow–Teller strength functions, and hence the $T_{1/2}$ and $P_n$, depend on the deformation. We report here on the measurements of the $\beta$-decay half-lives of nuclei between $^{36}$Mg ($N = 24$) and $^{48}$Ar ($N = 30$).

## 2. Experimental techniques and data analysis

The neutron-rich isotopes of interest were produced by the reaction of a 60 MeV/nucleon $^{48}$Ca$^{10+}$ primary beam on a 530 μm-thick Be target and selected using the doubly achromatic LISE3 spectrometer [16]. Five magnetic rigidity settings were employed in the present Letter (Table 1). Some of the nuclei were produced for different spectrometer settings, along with various neighboring nuclei at different count rates. We could, therefore, compare half-life measurements under different background conditions.

The particle identification was performed on an event-by-event basis using standard $\Delta E$-TOF identification techniques. The time-of-flight (TOF) was measured with respect to the cyclotron HF and by using 2 PPAC's located one meter upstream of the collection point. The energy-loss ($\Delta E$) provided for the de-

Table 1
Spectrometer settings

| Setting number | $^{48}$Ca beam intensity (μAe) | Be target thickness (μm) | Be degrader thickness (μm) | Rigidities $B\rho 1$–$B\rho 2$ (Tm) | Nucleus of interest | Rate (pps) | Other nuclei | Total rate (pps) |
|---|---|---|---|---|---|---|---|---|
| 1 | 1 | 747 | 220 | 2.857–2.468 | $^{43}$P | 0.4 | $^{43-45}$S, $^{41,42}$P, $^{39-42}$Si, $^{37-39}$Al, $^{36}$Mg | 10 |
| 2 | 2 | 747 | 1054 | 2.630–2.491 | $^{44}$S | 75 | $^{39-42}$P | 75 |
| 3 | 1.8 | 562 | 1054 | 2.851–2.451 | $^{46}$Cl | 150 | $^{44}$S | 155 |
| 4 | 1.8 | 679 | 536 | 2.886–2.667 | $^{47}$Cl | 0.6 | $^{44,45}$S, $^{46}$Cl | 3 |
| 5 | 1.8 | 689 | 536 | 2.734–2.521 | $^{48}$Ar | 3.5 | $^{47}$Ar, $^{46,47}$Cl | 10 |

termination of the charge ($Z$) of the fragments. The residual energy was measured in the double-side Si-strip implantation detector (DSSD). The last Si detector (500 μm) was used as a veto.

The nuclei were implanted in a 1 mm thick 48 × 48 mm$^2$ double-side Si-strip detector (DSSD) divided into 16 3 mm-wide strips in the horizontal and vertical directions. This segmentation allowed the location of the implanted nuclei to be determined which could then be correlated with the $\beta$-rays arising from the decay. An Al foil of adjustable thickness located upstream of the implantation point permitted the nuclei of interest to be implanted at the centre of the DSSD. The $\beta$-particles were detected using two 50 × 50 mm$^2$ plastic scintillators of thicknesses 500 and 1000 μm located 1 cm either side of the implantation detector. Because of the absorption of the low-energy $\beta$-rays in the thick Si implantation detector, the $\beta$-efficiency ($\epsilon_\beta$) depended on the beta energy ($E_\beta$). The absorption of the $\beta$-rays in the Si as a function of the $E_\beta$ was derived from a Monte Carlo simulation. The absolute $\beta$-efficiency was then obtained by adjusting this absorption curve to the value extracted from a measurement of the $^{35}$P decay and then checked using the decay of $^{17}$N.

The determination of the half-lives of the nuclei implanted in a continuous-beam mode requires time-correlation between the $\beta$-rays and the precursor implants to be made. When the total implantation rate of ions is small in compare with the measured half-life ($< 1/(5 \times T_{1/2})$), a very clean correlation is obtained. This condition was fulfilled in the spectrometer settings 1, 4 and 5 (Table 1). For higher implantation rates, as in settings 2 and 3, the additional requirement of a spacial correlation between the $\beta$-rays and precursor nuclei was required. As a test, the de-

Table 2
Half-lives deduced from the present and earlier works

| Nucleus | $T_{1/2}$ (msec) this work | $T_{1/2}$ (msec) literature |
|---|---|---|
| $^{36}$Mg | $3.9 \pm 1.3$ | |
| $^{37}$Al | $10.7 \pm 1.3$ | |
| $^{38}$Al | $7.6 \pm 0.6$ | |
| $^{39}$Al | $7.6 \pm 1.6$ | |
| $^{39}$Si | $47.5 \pm 2.0$ | |
| $^{40}$Si | $33.0 \pm 1.0$ | |
| $^{41}$Si | $20.0 \pm 2.5$ | |
| $^{42}$Si | $12.5 \pm 3.5$ | |
| $^{39}$P | $250 \pm 80$ | $160^{+300}_{-100}$[a]–$320 \pm 30$[b] |
| $^{40}$P | $125 \pm 25$ | $260 \pm 60$[a]–$146 \pm 10$[b] |
| $^{41}$P | $100 \pm 5$ | $120 \pm 20$[a]–$150 \pm 15$[b] |
| $^{42}$P | $48.5 \pm 1.5$ | $110^{+40}_{-20}$[a] |
| $^{43}$P | $36.5 \pm 1.5$ | $33 \pm 3$[c] |
| $^{44}$P | $18.5 \pm 2.5$ | |
| $^{43}$S | $282 \pm 27$ | $220^{+80}_{-50}$[a]–$260 \pm 15$[b] |
| $^{44}$S | $100 \pm 1$ | $123 \pm 10$[d] |
| $^{45}$S | $68 \pm 2$ | $82 \pm 13$[c] |
| $^{46}$S | $50 \pm 8$ | |
| $^{46}$Cl | $232 \pm 2$ | $223 \pm 37$[d] |
| $^{47}$Cl | $101 \pm 6$ | |
| $^{47}$Ar | $1250 \pm 150$ | $> 700$[c] |
| $^{48}$Ar | $475 \pm 40$ | |

[a] Ref. [17];  [b] Ref. [18];  [c] Ref. [19];  [d] Ref. [3].

termination of the half-life of $^{44}$S was made for two very different counting rates. In the first spectrometer setting, the $^{44}$S rate was 5.5 pps and was accompanied by 12 other isotopes, whereas in setting 2 the count rate was 75 pps with a purity of greater than 96%. Not only were the total counting rates different, but the other nuclei implanted and their yields were different. Half-lives of $99 \pm 2$ and $100.2 \pm 0.5$ msec, respectively, were deduced. The $\beta$-decay time-spectra
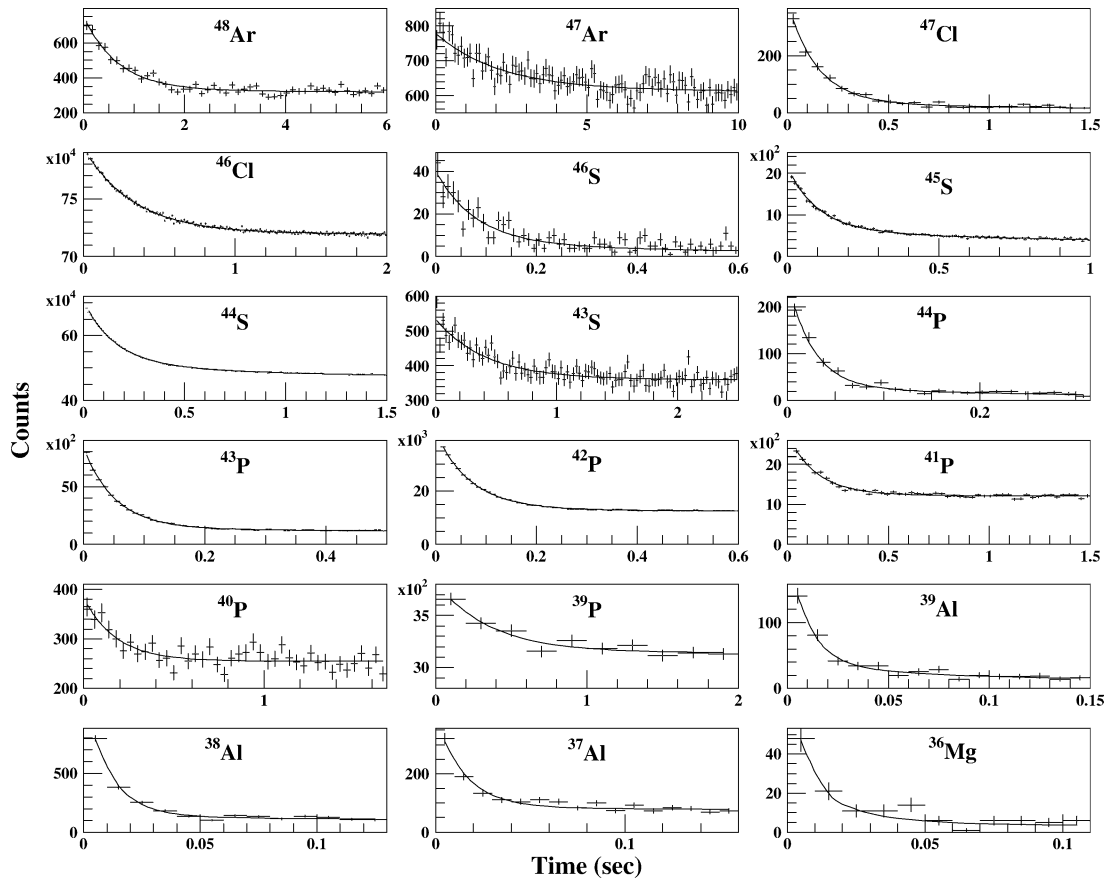
Fig. 1. Decay time spectra for isotopes of Ar, Cl, S, P, Al and Mg. The lines are the fits including the (un)known components arising from the decay of the daughter nuclei. The results for the Si isotopes are reported separately in Fig. 2.

are displayed in Fig. 1 for the isotopes of Ar, Cl, S, P, Al and Mg and in Fig. 2 for the Si isotopes. The half-lives extracted are listed in Table 2. The fitting procedure to determine the half-life includes several parameters: the number of implanted isotopes ($N_i$), the $\beta$-efficiency of the DSSD detector ($\epsilon_\beta$), the half-life ($T_{1/2}$) and delayed-neutron emission probabilities ($P_{xn}$) of the nucleus and its descendants, and the level of background. In case the periods or the $P_{xn}$-values of the descendants are not (well) known, the resulting uncertainties are included in the error bars. The $\epsilon_\beta$ value was checked to be coherent with that of nuclei with known $Q_\beta$. The background component, which mainly results from multiple links for each $\beta$-ray, is directly related to the total implantation rate and can be easily shown to be a constant. We note that if only the first $\beta$-particle detected following the implantation

is considered in the analysis the decay curve is distorted by the blocking of subsequent betas which may include that of interest. This effect is well reproduced by our detailed simulations.

## 3. Results and discussion

The half-lives derived from the present measurements are listed in Table 2 together with previously reported values. In all except one case ($^{42}$P), the present measurements are in good agreement with earlier work. In the case of $^{42}$P, the only previously reported measurement suffered from rather low statistics and encountered uncertainties in the determination of the background component [17,20]. As may be seen from the Table 2, the present study improves
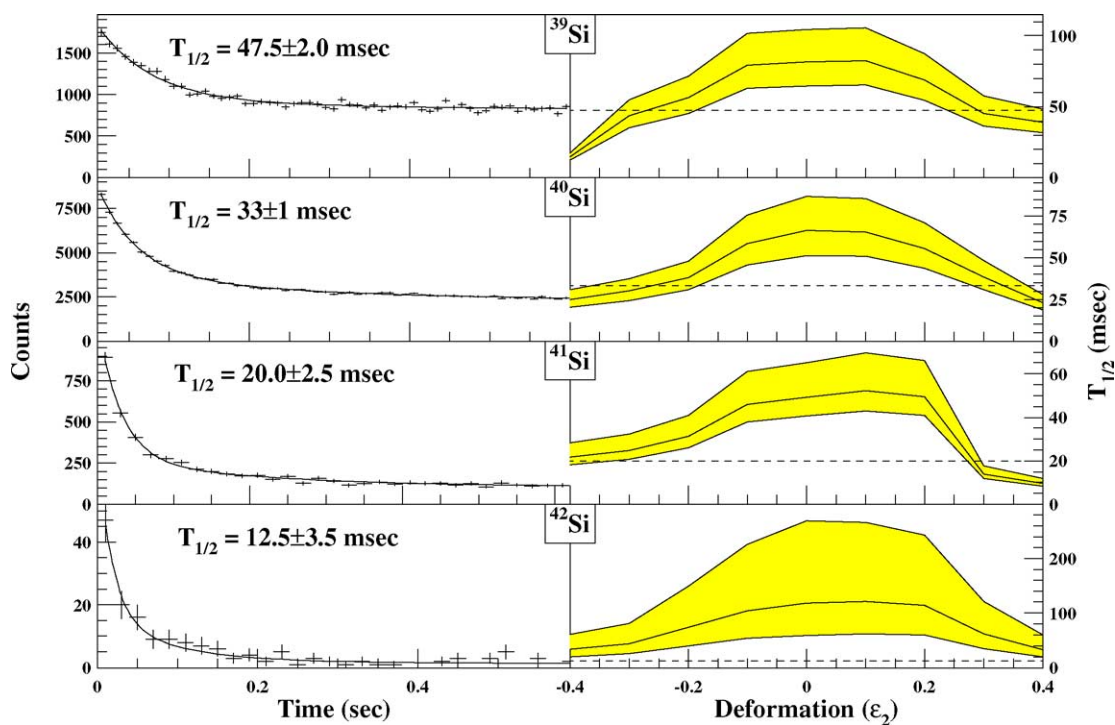
Fig. 2. Decay time spectra of $^{39-42}$Si (left) and corresponding QRPA calculations as a function of the deformation (right) where the experimental periods are reported as dashed lines. The sensitivity to the masses is reflected by the shaded areas.
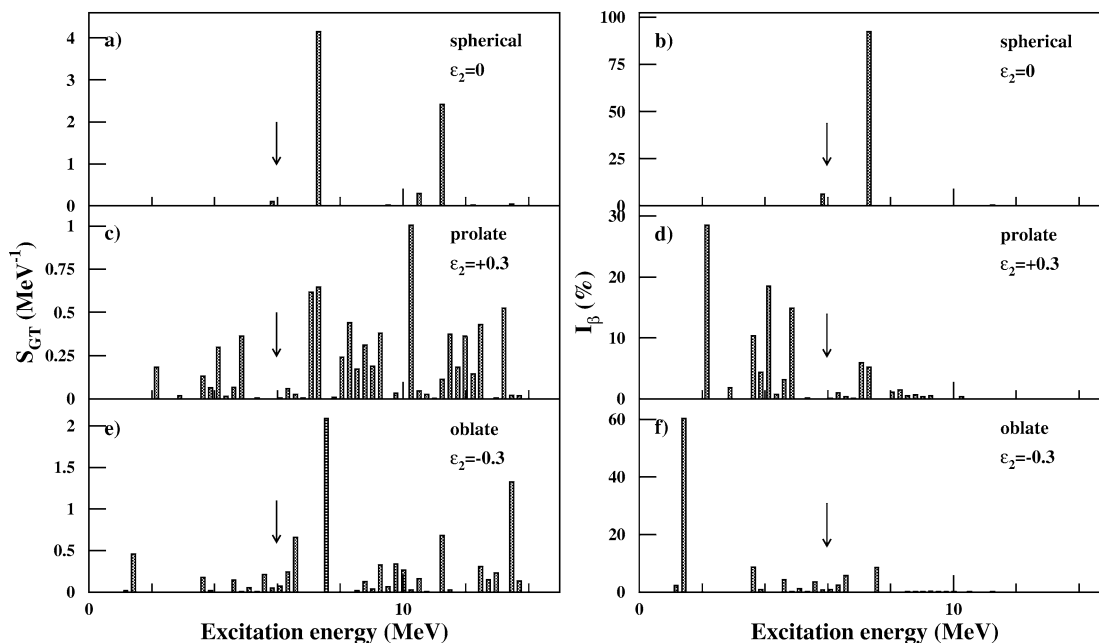


Fig. 3. Gamow–Teller strength function and corresponding intensity calculated for the decay of $^{42}$Si as a function of the excitation energy in $^{42}$P for different deformation ($\varepsilon_2$). The arrow indicates the one-neutron separation energy in $^{42}$P.

considerably on the precision of the earlier measurements. Moreover, some 12 half-lives have been measured for the first time (in the case of $^{47}$Ar only a lower limit could be established in Ref. [19]). As discussed below, perhaps the most significant new results are those obtained for the Si isotopic chain, whereby half-lives have now been established out to the $N = 28$ nucleus $^{42}$Si.

In order to gain some structural insight for the Si isotopes, we have used the QRPA theory of Möller and Randrup [21] in order to determine the half-lives for various quadrupole-deformation parameters, $\varepsilon_2$, between $-0.4$ and $+0.4$. We note that the QRPA model can only handle the same $\varepsilon_2$ values for the parent nucleus and states in the daughter. The essential ingredients of the calculations were as follows. For each $\varepsilon_2$ value, the wave functions of the parent and daughter nuclei were determined by solving the Shrödinger equation with a Folded–Yukawa potential. The Gamow–Teller $\beta$-strength functions ($S_{GT}(E^*)$) were then calculated for each state, $E^*$, in the daughter nucleus in order to deduce the $T_{1/2}$ values through the equation,

$$\frac{1}{T_{1/2}} = \int\limits_0^{Q_\beta} S_\beta(E^*).(Q_\beta - E^*)^5 \, dE^*.$$

The normalized intensity of the $\beta$-strength function ($I_\beta(E^*)$) was defined as,

$$I_\beta(E^*) = \frac{S_\beta(E^*).(Q_\beta - E^*)^5}{\int_0^{Q_\beta} S_\beta(E^*)(Q_\beta - E^*)^5 \, dE^*}.$$

Fig. 3(a) and (b) show the $S_{GT}(E^*)$ and $I_\beta(E^*)$ in the case of a spherical $^{42}$Si whereby the Gamow–Teller strength ($\nu f_{7/2} \to \pi f_{7/2}$) is confined essentially to a single transition at high excitation energy ($\sim 7$ MeV). As a result, the half-life value, $T_{1/2} = 264$ ms, is long. At large deformation, the $\beta$-strength becomes fragmented and is shifted to lower energies (Fig. 3(c)–(f)) due to the energy splitting of the $f_{7/2}$ proton orbital. Consequently, we find shorter half-lives: $T_{1/2} = 88$ ms for $\varepsilon_2 = +0.3$ and $T_{1/2} = 55$ ms for $\varepsilon_2 = -0.3$. These values are somewhat closer to the experimental half-life of $12.5 \pm 3.5$ msec. Moreover, part of the $\beta$-decay strength could occur through $\nu f_{7/2} \to \pi d_{5/2}$ first-forbidden (ff) transitions whose contribution has been calculated using the Gross the-

ory [22]. The ff-strength is a factor of about 26 weaker than the GT, but feeds states at very low excitation energy. As a consequence, the half-lives are shortened to 62.3 msec for $\varepsilon_2 = +0.3$ and to 44.1 msec for $\varepsilon_2 = -0.3$. Larger deformation would not change drastically the calculated half-lives (see Fig. 2).

As the half-lives are strongly $Q_\beta$ dependent, we have included the corresponding experimental uncertainties in the QRPA calculations of the $T_{1/2}$. In this context, we have taken the most recent experimental masses measured at GANIL for the neutron-rich Si isotopes [23]. Fig. 2 shows the results of the QRPA calculations as a function of the quadrupole deformation in the $^{39-42}$Si isotopes. The shaded area delimits the range of calculated half-lives given the experimental uncertainties on the $Q_\beta$. It is clearly evident that the experimental half-lives, represented as dashed lines in Fig. 2 can be reproduced only at large prolate or oblate deformations. Moreover, the deformation appears to increase from $|\varepsilon_2| \approx 0.2$ in $^{39}$Si to $|\varepsilon_2| \geqslant 0.3$ in $^{42}$Si. In addition to the half-lives, the $P_n$ is also sensitive to the deformation. In $^{42}$Si, the single-neutron separation energy ($S_n$) is very close to 6 MeV [23] and is indicated by the arrow in Fig. 3. In the spherical case, all the $\beta$-strength is located above the neutron-emission threshold, leading to a $P_n$ of 100%. The $P_n$ decreases to 72% for extreme prolate deformation ($\varepsilon_2 = +0.3$) and to 38% for the oblate case. Including the ff-transitions, the $P_n$ drops to 50% in the spherical and prolate cases and to 32% in the oblate case. It is clear that a measurement of the $P_n$ values of Si isotopes would give more insights into the deformation in this region.

From the comparison between the measured and calculated half-lives for the $^{42}$Si, we infer that it is strongly deformed. We note that the oblate deformation is in somewhat better agreement with the experimental value. This result also agrees with the observation at RIKEN of the $N = 29$ nucleus $^{43}$Si since its stability was interpreted as a possible signature of deformation in this region [24]. Indeed, the stability of this nucleus is in contradiction with the finite range drop model (FRDM) which predicts a single-neutron separation energy of $-1.68$ MeV, while the extended Thomas–Fermi plus Strutinsky integral method (ETFSI) suggests that $^{43}$Si is bound ($S_n = 0.6$ MeV). The main difference between the two approaches lies in the degree of deformation—the ETFSI predicting a larger deformation than the FRDM for the

Si isotopes around $N = 28$, indicating that the shell closure may have been overestimated by the FRDM.

This suggestion of strong deformation of the Si isotopes agrees also with Reinhard et al. [10] who have employed Hartree–Fock calculations and several effective interactions to study $^{44}$S. They have shown that the ground state configuration is very sensitive to the choice of the Skyrme force and concluded that deformed nuclei are found in the cases of a low $\nu f_{7/2}$–$p_{3/2}$ energy difference—i.e., a small $N = 28$ gap. On the other hand, the role of the protons has also been pointed out as a major contribution to the quadrupole collectivity in the neutron-rich S isotopes [5]. This may be traced to the small $\pi d_{3/2}$–$\pi s_{1/2}$ energy difference [14,25]. In $^{42}_{14}$Si, these orbitals are not yet filled, and we may expect a stabilization of the $Z = 14$ subshell closure. Moreover, experimental data from Ca($d$,$^3$He) reactions suggests [25,26] that the gap at $Z = 14$ between the $\pi d_{5/2}$ and $\pi s_{1/2}$ orbits is even larger for $N = 28$ (5.0 MeV) than for $N = 20$ (4.2 MeV). We thus believe that the protons do not contribute significantly to the deformation of the Si isotopes. Can we therefore conclude that the $N = 28$ shell gap vanishes in the neutron-rich Si isotopes?

In this context we note that Lalazissis et al. [7] predict a well deformed oblate minimum in the potential energy surface of $^{42}$Si. The evolution of the $N = 28$ isotones from a spherical $^{48}$Ca to the strongly oblate deformed $^{42}$Si was attributed to the reduction of the spherical $N = 28$ gap. In these relativistic mean field calculations, the spin–orbit potential is considerably reduced in neutron-rich drip-line nuclei; a reduction which is especially pronounced in the surface region. For the Mg isotopes, going from $N = 20$ to 28, the energy splitting decreases from 1.2 to 1.0 MeV for the $2p_{1/2}$–$2p_{3/2}$ spin–orbit partners and from 7.0 to 5.5 MeV for $1f_{5/2}$–$1f_{7/2}$. A similar reduction is observed in Ref. [11] where the spherical shell gap at $N = 28$ is 5.6 MeV in $^{34}$Si and 3.5 MeV in $^{42}$Si. Our QRPA calculations suggest a spherical gap around 3.4 MeV. The deformation in the Si isotopes could then be interpreted as a direct consequence of the modification of the spin–orbit force far from stability resulting from the increase of the surface diffuseness in such loosely bound neutron-rich nuclei. Then, $^{42}$Si may be the ideal candidate to measure experimentally the reduction of the $N = 28$ gap due to the reduction in the spin–orbit force far from stability.

In order to proceed further, it will be necessary to confirm more directly the deformation of the Si isotopes and to determine experimentally the size of the neutron-shell gap in $^{42}$Si. A direct measure of the deformation can be obtained from Coulomb excitation, but such an experiment require much higher beam intensity than presently available. In beam $\gamma$-spectroscopy measurements can be undertaken at relatively low intensities (see, for example, Ref. [27]) and may permit the energies of the $2^+$ and $4^+$ states to be established. In the next few years, second-generation radioactive beam facilities will hopefully provide a $^{42}$Si beam with sufficient intensity to perform a $(d, p)$ reaction measurement, thus providing access to the single-particle energies in $^{43}$Si.

## 4. Conclusions

We have reported here on measurements of the beta-decay half-lives of very neutron-rich nuclei in the region of the $N = 28$ shell closure. Some 22 half-lives have been determined, including 12 for the first time. In the cases for which measurements already existed the precisions have been considerably improved. Through comparison with QRPA calculations we conclude that the neutron-rich Si isotopes are deformed. In the case of $^{42}$Si a deformation (possibly oblate) of $|\varepsilon_2| \geqslant 0.3$ was deduced. Links to a possible weaking in the spin–orbit potential have been discussed. More experimental work is clearly required to confirm the suggestions made here. In particular, a direct measurement of the deformations would be highly desirable, although probably not feasible in the near future. Measurements of the delayed-neutron emission probabilities and the position of the first $2^+$ states are, however, feasible and can be expected to be undertaken in the very near future. Similarly, the decay schemes of the nuclei investigated here would also provide constraints on our interpretation of their structure. Future papers will report on the results of the analysis of beta-gamma and beta-neutron decay data sets obtained in parallel with the work described here.

## References

[1] H. Scheit, et al., Phys. Rev. Lett. 77 (1996) 3967.
[2] T. Glasmacher, et al., Phys. Lett. B 395 (1997) 163.
[3] O. Sorlin, et al., Phys. Rev. C 47 (1993) 2941.
[4] F. Sarazin, et al., Phys. Rev. Lett. 84 (2000) 5062.
[5] D. Sohler, et al., Phys. Rev. C 66 (2002) 054302.
[6] Zs. Dombradi, et al., Nucl. Phys. A 727 (2003) 195.
[7] G.A. Lalazissis, et al., Phys. Lett. B 418 (1998) 7.
[8] G.A. Lalazissis, et al., Phys. Rev. C 60 (1999) 01431.
[9] T.R. Werner, et al., Phys. Lett. B 335 (1994) 259;
     T.R. Werner, et al., Nucl. Phys. A 597 (1996) 327.
[10] P.G. Reinhard, et al., Phys. Rev. C 60 (1999) 014316.
[11] S. Péru, M. Girod, J.F. Berger, Eur. Phys. J. A 9 (2000) 35.
[12] R. Rodriguez-Guzman, et al., Phys. Rev. C 65 (2002) 024304.
[13] V.E. Oberacker, et al., Phys. Rev. C 68 (2003) 064302.
[14] J. Retamosa, et al., Phys. Rev. C 55 (1997) 1266.
[15] S. Nummela, et al., Phys. Rev. C 63 (2001) 044316.
[16] A.C. Mueller, R. Anne, Nucl. Instrum. Methods Phys. Res. B 56 (1991) 559.
[17] M. Lewitowicz, et al., Nucl. Phys. A 496 (1989) 477.
[18] J.A. Winger, et al., in: B.M. Sherrill, D.J. Morissey, C.N. Davids (Eds.), Proceedings of ENAM98, Exotic Nuclei and Atomic Masses, AIP Conf. Proc. 455 (1998) 606.
[19] O. Sorlin, et al., Nucl. Phys. A 583 (1995) 763.
[20] M. Lewitowicz, private communication.
[21] P. Möller, J. Randrup, Nucl. Phys. A 514 (1990) 1.
[22] K. Takahashi, et al., Prog. Theor. Phys. 47 (1972) 1500;
     K. Takahashi, et al., At. Data Nucl. Data Tables 12 (1973) 101.
[23] H. Savajols, private communication.
[24] M. Notani, et al., Phys. Lett. B 542 (2002) 49.
[25] P.D. Cottle, et al., Phys. Rev. C 58 (1998) 3761.
[26] P. Doll, et al., Nucl. Phys. A 263 (1976) 210.
[27] M. Stanoiu, et al., in: P. Fallon, R. Clark (Eds.), Proceedings Frontiers of Nuclear Structure, AIP Conf. Proc. 656 (2003) 311.